Dipole Layer Formation by Surface Segregation of Regioregular Poly(3-alkylthiophene) with Alternating Alkyl/Semifluoroalkyl Side Chains

ARTICLE *in* CHEMISTRY OF MATERIALS · AUGUST 2011

Impact Factor: 8.35 · DOI: 10.1021/cm2018423

CHEMISTRY OF MATERIALS

ARTICLE

pubs.acs.org/cm

Dipole Layer Formation by Surface Segregation of Regioregular Poly(3-alkylthiophene) with Alternating Alkyl/Semifluoroalkyl Side Chains

Yanfang Geng,[†,‡] Qingshuo Wei,[§,⊥] Kazuhito Hashimoto,[*,†,§] and Keisuke Tajima[*,†,§]

[†]Department of Applied Chemistry, School of Engineering, The University of Tokyo, 7-3-1 Hongo, Bunkyo-ku, Tokyo 113-8656, Japan

[§]HASHIMOTO Light Energy Conversion Project, ERATO, Japan Science and Technology Agency (JST)

[‡]Department of Materials, School of Materials, Beijing Institute of Technology, 5 South Zhongguancun Street, Haidian District, Beijing 100081, P. R. China

Supporting Information

ABSTRACT: A regioregular poly(3-alkylthiophene) with alternating alkyl/semifluoroalkyl side chains (P3DDFT) spontaneously segregates on the surface of poly(3-dodecylthiophene) (P3DDT) during a spin-coating process and forms a thin fluoroalkyl layer with a thickness of less than 3 nm. This surface layer is as dense as fluoroalkyl-based self-assembled monolayers (SAMs) on metals, as demonstrated by angle-dependent X-ray photoelectron spectroscopy and water contact angle measurements. The semifluoroalkyl chains aligned at the air/solid interface form a large molecular dipole moment that continuously shifts the ionization energy by as much as +1.8 eV depending on the surface density of P3DDFT. This can be a novel approach to controlling the energy-level alignment at organic/(in)organic interfaces, analogous to the work function shifts of metals induced by the formation of SAMs.

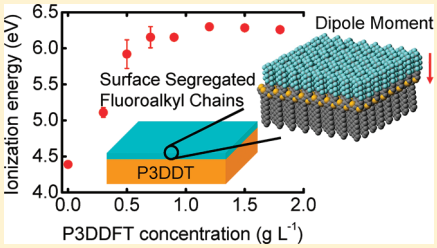

KEYWORDS: conjugated polymers, organic electronics, structure−property relationship, thin films, self-assembly

INTRODUCTION

Electronic and optoelectronic devices using organic materials such as organic field-effect transistors (OFETs),[1] light-emitting diodes (OLEDs),[2,3] and photovoltaic devices (OPVs)[4] have been drawing much attention. The surface and interface properties of organic semiconductors are of particular importance to achieve high performance of the devices,[5] since they largely affect the flow of charge carriers *across* or *along* material interfaces. For example, the charge injection barrier at metal/semiconductor interfaces is one of the most important issues in OLEDs, and many researches have been focusing on the reduction in the height of this barrier by modifying such interfaces.[6] The open circuit voltage (V_{OC}) and charge separation probability of OPVs are also largely affected by the properties of the material interface, such as the energy level offset of the electron donor and the type of acceptor material.[7] In OFETs, permanent dipole moments induced by self-assembled monolayers (SAMs) at a semiconductor/dielectric interface could affect the charge accumulation at the interface, resulting in a change in driving gate voltage.[8,9]

The science of SAMs on metals or oxides based on small molecules is well-established: it relies on specific chemical interactions between surfaces and modifiers such as thiol−metal or Si−O bonds. However, there is limited general technology available for modifying the surfaces and interfaces of organic semiconductors, especially polymer semiconductors, to fine-tune their electronic properties.[10] The evaporation of molecules in vacuum can produce a well-defined material interface but cannot be applied to polymer materials. The successive spin coating of soluble materials on organic films is quite difficult to apply to the preparation of multilayer structures because solvents dissolve or damage the underlying layers.

The surface modification of polymeric materials by segregation of the materials with a low surface energy such as fluoroalkylated or silicone compounds is of great interest in the field of materials science because of its important applications as, for example, nonadhesive biomaterials and antidirt coatings.[11−15] Recently, we have extended this approach to modifying the surface of organic semiconductor films.[16−18] We showed that fullerene derivatives with fluoroalkyl chains (FC_n) spontaneously form a monolayer on the surface of a nonfluorinated fullerene derivative (PCBM) film during the coating process, and named it surface segregated monolayer (SSM). Aligned fluorocarbon chains form a surface dipole moment that changes the surface energy structure of PCBM films. We also showed that SSM can be utilized as a buffer layer at organic/metal interfaces in OPVs, possibly by suppressing charge carrier recombination.[17] Extending the concept of SSM to semiconducting polymer films would be of great value in the field of organic electronics.

Received: June 28, 2011
Revised: August 15, 2011
Published: August 30, 2011

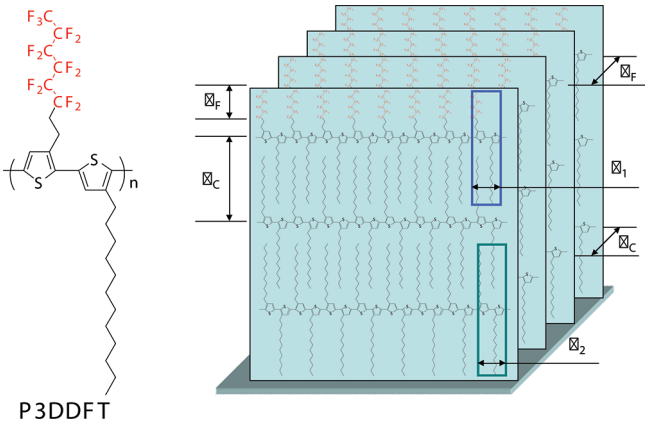

Figure 1. Molecular structure of P3DDFT and schematic representation of surface-segregated P3DDFT layer on the surface of P3DDT bulk film. L_F is the thickness of the fluorocarbon layer, L_C is the interlayer distance, d_F and d_C are the distances between π-plane of P3DDFT and P3DDT, respectively, and d_1 and d_2 are the lengths of the bisthiophene repeating units in P3DDFT and P3DDT, respectively.

The effect of fluorination on the properties of semiconductors has been attracting much attention to the application in organic electronics. Polythiophenes with perfluorinated and semifluoalkyl alkyl side chains have shown promising photoelectronic properties. Materials with amphiphilic (hydrophobic and fluorophilic) side chains[19,20] have been reported to form highly ordered lamellar structures in bulk. However, there are as yet no reports on the segregation behaviors of these polymers on the surface of semiconducting polymer films.

It has been suggested by both direct surface analysis and indirect electronic property measurement that the surface of spin-coated films of regioregular poly(3-alkylthiophene)s has an "edge-on" orientation with alkyl side chains sticking out in the air direction, probably owing to the low surface energy of side chains and stabilization by the $\pi-\pi$ stacking of their backbones.[21−25] Deducing from this possible surface structure, an alternating substitution of alkyl chains to semifluoroalkyl chains in the 3-position of regioregular poly(3-alkylthiophene)s could result in the orientation of semifluoroalkyl side chains at the surface (Figure 1). The resulting surface layer could have high order and density, resulting in a large modulation of the surface properties of organic semiconductor films. Energy level control by adjusting the side chain dipole moment of poly(3-alkylthiophene)s has recently been proposed on the basis of theoretical calculations.[26]

In this paper, we report the surface segregation behavior of regioregular poly[4′-dodecyl-3-(1H,1H,2H,2H-perfluorooctyl)-2,2′-bithiophene] (P3DDFT) with alternating substitution of semifluoroalkyl and alkyl chains investigated by X-ray photoelectron spectroscopy (XPS). The surface coverage of a P3DDFT layer on poly(3-dodecylthiophene) (P3DDT) films has been changed by simply changing the mixing ratio of the blend solution. The energy structures at the surfaces were examined by ultraviolet photoelectron spectroscopy (UPS),[27−29] and the effect of surface segregated layers on the ionization energy of the films was investigated.

EXPERIMENTAL SECTION

Regioregular P3DDFT was synthesized via the Grignard metathesis (GRIM) reaction followed by Ni-catalyzed polymerization.[30] The number-average molecular weight (M_n) and polydispersity index (PDI) of P3DDFT were 14 600 and 1.52, respectively. Regioregular poly(3-dodecylthiophene) (P3DDT) was synthesized following a typical method.[30] Its M_n was 23 600 and its PDI was 1.11.

Glass, indium−tin oxide (ITO)-coated glass and silicon substrates (highly doped n-type wafer (<0.02 Ω cm) with 300 nm thermally grown silicon dioxide, rms of roughness: < 0.2 nm) were sequentially cleaned by ultrasonication in detergent, water, acetone, and isopropanol. Just before use, the substrates were exposed to UV−O_3 for 30 min.

X-ray photoelectron spectroscopy (XPS) was performed on an AXIS-ULTRA DLD spectrometer (Kratos Analytical Ltd.) and a JPS-9010MC XPS spectrometer. Al K_α radiation was used in all the measurements. The films were prepared on ITO-coated glass substrates by spin coating (3000 rpm/30 s) the solutions with various concentrations of P3DDFT (0.3−1.8 g L^{-1}) and a fixed concentration of P3DDT at 10 g L^{-1}. The solutions were heated to around 110 °C during the spin-coating process because the introduction of semifluoroalkyl chains makes P3DDFT less soluble in the solvents at room temperature. Before the measurements, the films were placed under high vacuum for 2 h until the pressure dropped down to 1.0 × 10^{-7} Pa. The fluorine 1s (F 1s, 687 eV) and carbon 1s (C 1s, 283 eV) peaks were used for the characterization. To obtain the XPS depth profile, the blend films were prepared from the solutions with the concentrations of 0.7 mg mL^{-1} and 1.5 mg mL^{-1} on the glass substrates. Each sample was etched using an argon ion etcher at an acceleration voltage of 500 V.

Ultraviolet photoelectron spectroscopy (UPS) was recorded on the same sample with XPS measurements using an AXIS-ULTRA DLD spectrometer (Kratos Analytical Ltd.) with He (I) excitation of 21.2 eV and a pass energy of 5 eV. For each UPS measurement, a bias voltage of approximately −6.3 V was applied to the sample substrates using a battery.

X-ray diffraction (XRD) analysis and X-ray reflectivity (XRR) analysis were performed on a Rigaku Smartlab X-ray diffractometer. Monochromatized CuKα radiation (λ = 0.154 nm) was generated at 45 kV and 200 mA. The samples for XRD were prepared by dropcasting and evaporating a cholorobenzene solution of P3DDT and P3DDFT on glass substrates followed by annealing the resulting films at 150 °C (P3DDT) and 230 °C (P3DDFT) for 1 h, respectively. In-plane measurement was preformed with the incident angle of 0.200°. The details can be found in our previous report.[30]

The static contact angle of distilled water on the pristine P3DDT and blend films were measured on a Kyowa CA-X contact angle meter at room temperature. The films were prepared on the silicon substrates with the same fabrication method for the XPS measurements.

The one-dimensional (1D) periodic DFT calculations were performed using Gaussian 03 software package with B3LYP functional and 6-31G(d) basis set. The molecular structures including translation vectors have been optimized by minimizing the energy. The number of k-points was 43 for both the periodic calculations.

RESULTS AND DISCUSSION

F/C Atomic Ratios on Surface. The surface segregation behavior of P3DDFT in the blend films of P3DDT and P3DDFT was monitored by XPS. The F/C atomic ratios of the surface were calculated from the peak intensities and plotted in Figure 2 as a function of the P3DDFT concentration in the solutions. The F/C atomic ratios calculated from the polymer compositions of the mixed solutions, which represent the expectations for homogeneously mixed films, are also shown in Figure 2 for comparison. The surface F/C ratios of the films were much higher than the calculated ratio of the solution for all the concentrations. This indicates the segregation of P3DDFT to the film surface during

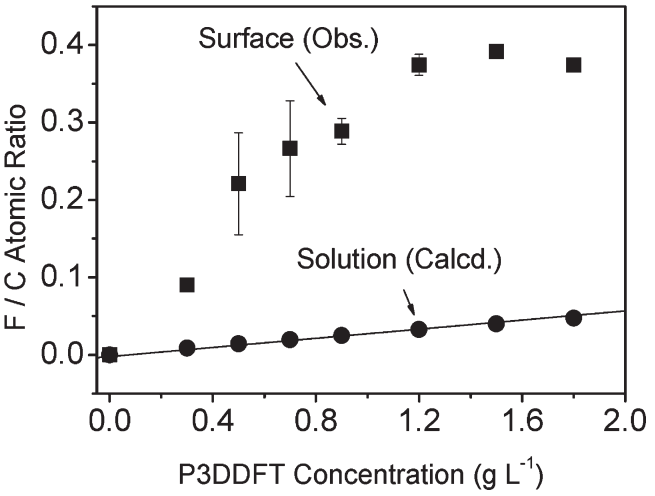

Figure 2. F/C atomic ratio on the surfaces of P3DDFT/P3DDT thin films (filled squares) measured by XPS and plotted as a function of P3DDFT concentration of the spin-coating solutions and F/C ratios calculated from the polymer compositions of the solutions (filled circles).

the spin-coating process. In the lower-P3DDFT-concentration region, the F/C atomic ratio almost linearly increased with the concentration of P3DDFT. At a P3DDFT concentration of around 0.9 g L^{-1}, the F/C atomic ratio increased up to approximately 0.38 and saturated above that. This saturation behavior was also observed in our previous work on the fullerene-based SSM (FC_n/PCBM), but the F/C atomic ratio of P3DDFT/P3DDT in the saturated region is approximately three times larger than that of FC_n/PCBM (0.13).[16] This higher concentration of F atom on the surface can be explained by the fact that FC_n has a larger footprint for each fluoroalkyl chain than P3DDFT, because of the larger volume of its fullerene part.

Comparison with Calculated F/C Atomic Ratio. If it is assumed that a uniform monolayer forms on the surface at the saturated concentration, F/C atomic ratio could be calculated. For a simple bilayer model, the XPS intensity of the atoms in the films and the substrates can be described as[31,32]

$$\frac{I_f}{I_s} = \frac{I_f^0 X_f}{I_s^0 X_s}\left[\exp\left(\frac{d}{\lambda_s \cos\theta}\right) - \exp\left(\frac{d\lambda_f - d\lambda_s}{\lambda_f \lambda_s \cos\theta}\right)\right] \quad (1)$$

where d is the thickness of the film, I_f and I_s are the XPS peak intensities of the atoms in the film and substrate, respectively, X_i are the local concentrations of the element i, λ_i are the attenuation lengths of photoelectrons, θ is the takeoff angle and I_i^0 are the atomic relative sensitivity factors (RSFs) of the element i, which are given by the manufacturer of the XPS spectrometer.

A model with a densely packed P3DDFT layer on the P3DDT film is constructed as shown in Figure 1 according to X-ray diffraction analysis on the polymer films previously reported.[30] The thickness of the fluorocarbon layer L_F (d in eq 1) is estimated to be 0.75 nm, assuming that the layer has extended chains and a vertical orientation. The length of nonfluorinated chains L_C is determined to be 2.6 nm ($2\theta = 3.40°$) by in-plane X-ray diffraction of the P3DDT pristine film. Two hydrocarbons between the fluorocarbon chain and the thiophene ring were ignored for simplicity. The RSFs of F 1s and C 1s are 1.000 and 0.278, respectively. The attenuation lengths (λ) of F 1s and C 1s

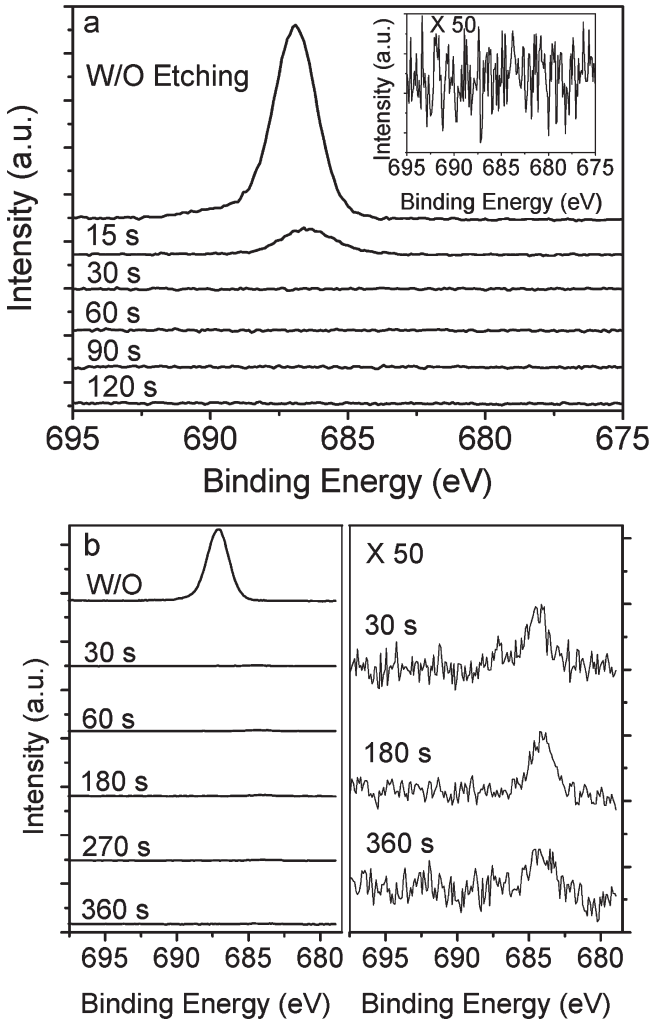

Figure 3. (a) XPS depth profile in F 1s region of an as-cast film with a P3DDFT concentration of 0.7 g L^{-1} without etching and after etching for 15, 30, 60, 90, and 120 s. Inset: an enlarged view of F 1s region after 30 s etching. (b) XPS depth profile in F 1s region of an as-cast film with a P3DDFT concentration of 1.5 g L^{-1} without etching and after etching. Right panel: an enlarged view of the same region after etching for 30, 180, and 360 s.

are 2.8 and 3.8 nm, respectively, according to a previous report.[33] Here, the numbers of atoms in the unit cell are considered as the local concentrations of the elements. There are 13 F atoms in the fluorocarbon layer and 32 C atoms in the nonfluorinated layer (two dodecyl chains and two thiophene rings) per repeating unit. The takeoff angle is set to 0°, as in the measurement. Thus, the calculated F/C ratio based on the model was

$$\frac{I_f}{I_s} = \frac{13/0.75}{32/2.6}\left[\exp\left(\frac{0.75}{3.8}\right) - \exp\left(\frac{0.75 \times (2.8 - 3.8)}{2.8 \times 3.8}\right)\right] = 0.40. \quad (2)$$

This value is close to the observed one (0.38). This result suggests that at high concentrations above the saturated point, the surface is almost completely covered by fluoroalkyl chains of P3DDFT.

XPS Depth Profiles. XPS depth profiles were used to further confirm surface segregation. P3DDT solution with 0.7 g L^{-1} P3DDFT (which is below the saturated concentration) was spin

dx.doi.org/10.1021/cm2018423 |Chem. Mater. 2011, 23, 4257–4263

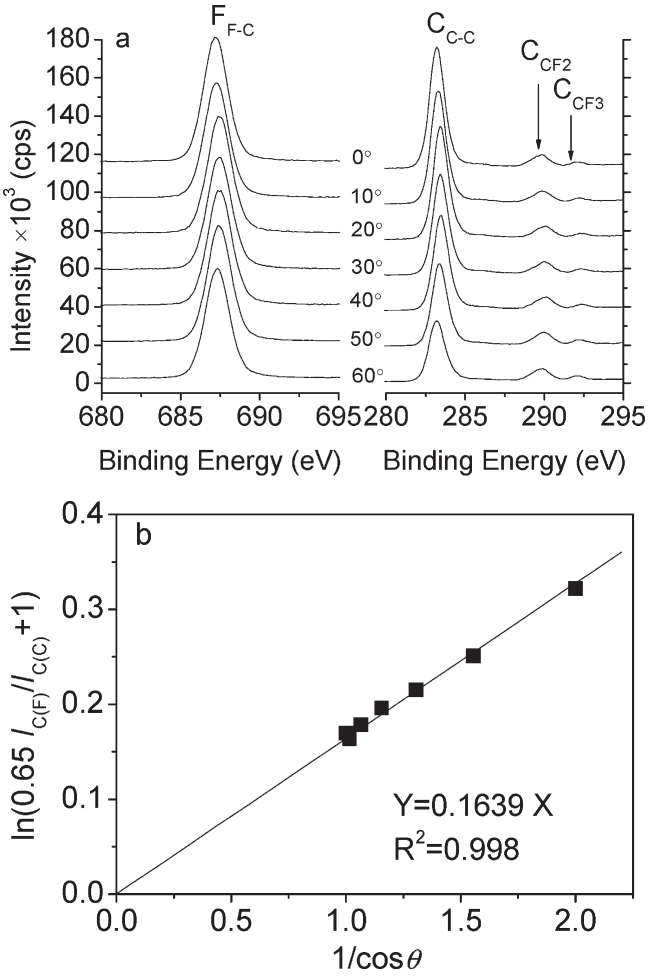

Figure 4. (a) F 1s and C1s regions of XPS profiles of the P3DDT film prepared with 0.7 g L^{-1} P3DDFT in the solution with different takeoff angles. (b) 1/cos θ vs ln(0.65 × $I_{C(F)}/I_{C(C)}$+1) plot for P3DDFT surface layer using C 1s peaks.

coated on a flat glass substrate. The surface of the film was etched with an argon ion beam. F 1s and C 1s from the film and Si 2p from the substrate were monitored. The F 1s region on the surface after etching for the designated time is shown in Figure 3a. After 15 s of etching from the surface, F 1s peak intensity decreased drastically with a slight shift that might be attributed to charging up of the surface by the etching. After 30 s, the F 1s peak disappeared completely. There were no F 1s peaks observed inside the film, indicating that all P3DDFT segregated at the surface (see the inset). The thickness of the film determined by X-ray reflectivity (XRR) and UV−visible absorbance analysis (see the Supporting Information) was 48.9 nm and the time of the entire film etching was approximately 480 s, determined by the appearance of Si 2p peaks and the disappearance of C 1s peaks. The etching rate was estimated as 0.1 nm s^{-1}. Therefore, the thickness of the layer containing fluorine can be estimated as less than 3 nm, which indicates that P3DDFT segregated on the surface as a very thin layer, possibly a monolayer.

The XPS depth profiles of the film with a P3DDFT concentration of 1.5 g L^{-1} (which is above the saturated concentration) are shown in Figure 3b. A distinct F 1s peak was observed on the surface, indicating that P3DDFT segregated on the surface

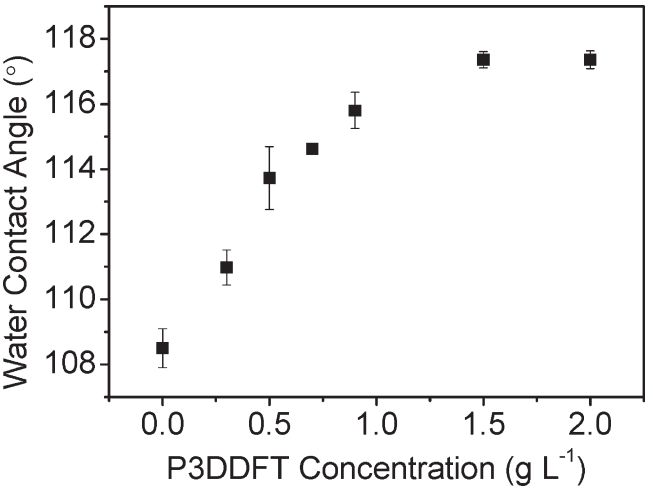

Figure 5. Static water contact angles on the surfaces of pristine P3DDT and blend P3DDT/P3DDFT films plotted as a function of P3DDFT concentration in the spin-coating solutions.

during spin coating. However, in contrast to the results for the low concentration, F 1s peaks with almost constant intensities were observed in the bulk of the film. This result indicates that a small amount of P3DDFT remained in the bulk of film above the saturated concentration.

Considering the XPS results above, the surface segregation behavior of P3DDFT could be explained as follows: at a lower concentration of P3DDFT in the solution (below ca. 0.9 g L^{-1}), all the added P3DDFT segregated to the surface to form the mixed surface layer of P3DDFT and P3DDT. Above the saturated concentration, the surface was completely covered with a P3DDFT layer and the residual P3DDFT remained in the bulk of the film. Note that this simple picture does not largely contradict the ratio of the polymers in the mixture solutions. The film thickness is about 50 nm for the P3DDFT concentration of 0.9 g L^{-1} and the monolayer thickness could be estimated as 3.4 nm (see Figure 1), which gives a P3DDFT/P3DDT volume ratio of 0.073 in the film. This corresponds to a P3DDFT concentration of 0.73 g L^{-1} in the solution, assuming the same density for the polymers. Therefore, the segregation of all P3DDFT to the surface is possible below this concentration. Above this concentration, excess P3DDFT could exist in the solutions, which might either be driven out during the spin coating or remain in the bulk of the film, as observed in the XPS depth profile.

Length of Fluorocarbon Chain. To quantitatively calculate the thickness of the fluorocarbon layer on the surface, we performed angle-dependent XPS (ADXPS). Figure 4a shows the F 1s and C 1s regions of XPS at different takeoff angles. Note that the C 1s peaks of fluorinated and nonfluorinated carbons were separately observed at 290−292 and 283 eV, respectively. As the angle increased, the peak intensities of F 1s and fluorinated C 1s did not change, while that of nonfluorinated C 1s decreased. This result qualitatively indicates that fluorocarbon chains are exposed to the air/film interface, whereas the alkylthiophene part exists underneath.

The thickness of the fluorinated carbon layer L_F on the surface was quantitatively determined by ADXPS from the same model for the calculation of surface density.[31] To simplify the calculation, the C 1s peaks of CF_2 (289.7 eV), CF_3 (291.8 eV), and

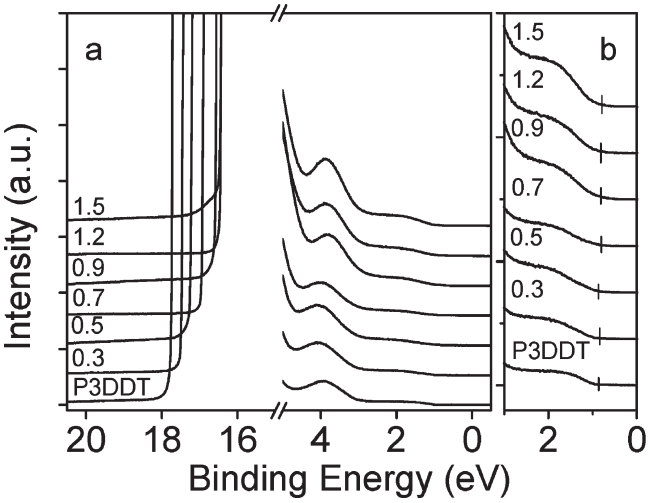

Figure 6. (a) UPS profiles of the as-cast films of P3DDT and P3DDFT/P3DDT with various concentrations of P3DDFT and (b) blow-up of the low binding energy region with marks at the edge of HOMO levels.

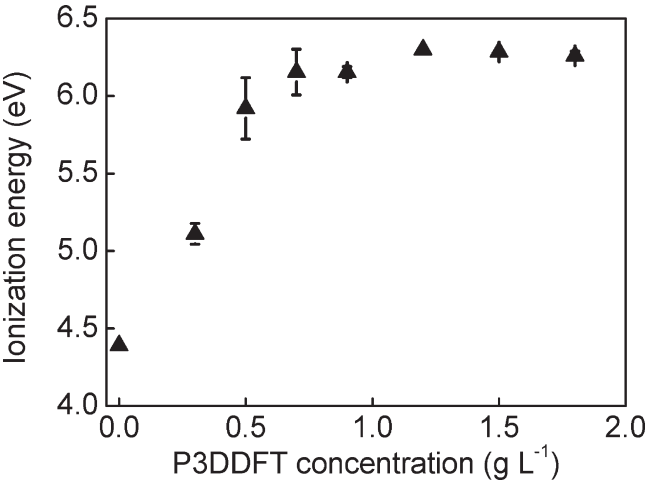

Figure 7. Ionization energy of the P3DDFT/P3DDT films plotted as a function of the concentration of P3DDFT in the spin-coating solution.

nonfluorinated carbons (283 eV) were used. Equation 1 can be transformed to

$$\ln\left(\frac{I_{C(F)}}{I_{C(C)}}\frac{I^0_{C(C)}X_{C(C)}}{I^0_{C(F)}X_{C(F)}}+1\right)=\frac{d}{\lambda_C\cos\theta} \quad (3)$$

where $I_{C(F)}$ and $I_{C(C)}$ are the intensities of the C 1s peak of the fluorocarbon layer and C 1s peak of nonfluorinated carbons, respectively. Since the same element was used for the measurement, the ratio of the sensitivity factors $I^0_{C(C)}/I^0_{C(F)}$ was 1. $X_{C(F)}$ and $X_{C(C)}$ are the local concentrations of the corresponding atoms. There are 6 fluorinated carbon atoms in the fluorocarbon layer and 32 nonfluorinated carbon atoms (two dodecyl chains and two thiophene rings) per repeating unit. Thus, $I^0_{C(C)}X_{C(C)}/I^0_{C(F)}X_{C(F)} = 0.65$. The thickness of the film can be obtained by plotting $\ln(0.65\ I_{C(F)}/I_{C(C)}+1)$ as a function of $1/\cos\theta$, as shown in Figure 4b. The bilayer model assumed here fits the experimental data very well, suggesting the validity of the model. The thickness L_F (d) obtained from the slope of the fitting line is 0.62 nm (with C 1s attenuation length of 3.8 nm).[33] This value is close to the estimated length of the fluorocarbon (0.75 nm), indicating that the P3DDFT thin layer on the surface can be regarded as a monolayer.

Static Water Contact Angle. Static water contact angles on the polymer films were measured; these angles are sensitive to the chemical composition and physical structure of the surface.[34] Contact angle is plotted in Figure 5 as a function of the concentration of P3DDFT in the solution. The angle increased as the concentration of P3DDFT increased and saturated at around 0.9 g L^{-1}. This tendency is similar to that of the surface F/C atomic ratio. This could be attributed to the gradual exchange of alkyl chains for the more hydrophobic fluoroalkyl chains on the film surface as the P3DDFT concentration increased. An average angle of 117° was observed above the saturated concentration. This value is similar to that of $CF_3(CF_2)_7SH$ SAMs on gold (117°) and slightly lower than that of $CF_3(CF_2)_7(CH_2)_{11}SH$ SAM on gold (121°).[35,36] However, it is larger than that of $CF_3(CF_2)_7(CH_2)_2Si$ SAMs on silicon (108.8−109.6°).[8,37] The contact angle difference between the P3DDT surface and the surface above the saturation was about 9°, which is similar to the difference between $CH_3(CH_2)_{17}Si$ and $CF_3(CF_2)_7(CH_2)_2Si$ SAMs on silicon.[38] The effect of surface roughness could be neglected, since the roughness of the films is not high enough to induce a difference in water contact angle even at high P3DDFT concentrations, as confirmed by AFM (i.e., the roughness factors ~1, see the Supporting Information). The result supports the formation of densely packed, aligned fluoroalkyl chains on the polymer surface similarly to the SAMs on metals or oxides.

Calculation of Surface Density. The maximum surface density of P3DDFT on P3DDT films in the lateral direction was calculated based on a densely packed surface model (Figure 1). The $\pi-\pi$ distance in P3DDT (d_C = 3.84 Å, 2θ = 23.13°) and P3DDFT (d_F = 3.80 Å, 2θ = 23.38°) was obtained from the corresponding pristine films by in-plane X-ray diffraction measurement. The cell length in the direction of polythiophene chains in P3DDT (d_2 = 7.86 Å) and P3DDFT (d_1 = 7.85 Å) was obtained from the translation vectors in the density functional theory (DFT) calculations. The calculated surface densities of the side chains were 5.50×10^{-10} mol cm^{-2} for P3DDT and 5.56×10^{-10} mol cm^{-2} for P3DDFT, assuming an "edge-on" orientation. The fluoroalkyl chain density of the surface is about three times higher than that of FC_n ($1.6-1.7 \times 10^{-10}$ mol cm^{-2}) and comparable to that of SAMs of fluoroalkylthiol on Au (5.3×10^{-10} mol cm^{-2}).[39−42] These estimations indicate that the fluoroalkyl chains of P3DDFT could form a layer on the surface as densely packed as SAMs, as suggested by the large water contact angle.

Ultraviolet Photoelectron Spectroscopy (UPS). UPS was carried out to confirm the dipole moment formation by P3DDFT layers that are spontaneously segregated on the surface during spin coating. The UPS profiles of a pristine P3DDT film and films with various concentrations of P3DDFT layers on the surface are shown in Figure 6 and Figure S3. There is a large shift of the high binding energy cutoff of the UPS spectra but the edges of HOMO level are similar, indicating that P3DDFT on the surface markedly changes the vacuum level of the surface.

Ionization energy (IE) was determined from the width of the UPS profiles (from the edges of HOMO level to the high binding energy cutoff) and is plotted against the concentration of P3DDFT in the solutions in Figure 7. The surface-segregated

dx.doi.org/10.1021/cm2018423 |Chem. Mater. 2011, 23, 4257–4263

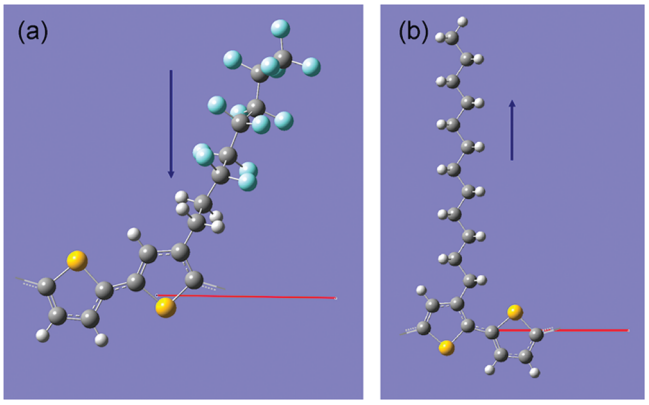

Figure 8. Optimized structures of the model compounds for (a) P3DDFT and (b) P3DDT obtained by density functional theory (DFT) calculations (Gaussian 03 package with B3LYP functional and 6-31G(d) basis set). To simulate the symmetry breaking at the surface, we removed the alkyl chains pointing away from the surface in the models. The 1D periodic structure is assumed to be along the polythiophene chain and red arrows indicate the translation vectors (7.85 and 7.86 Å for P3DDFT and P3DDT, respectively). Blue arrows indicate the calculated dipole moments (1.75 and 0.84 D for P3DDFT and P3DDT, respectively).

P3DDFT layers increased the IE proportional to the concentration of P3DDFT up to about 0.75 g L^{-1}. Above this concentration, IE saturated at 6.2 eV. This saturated concentration was a little lower than the point at which the density of P3DDFT obtained by XPS and water contact angle saturated (ca. 0.9 g L^{-1}). The maximum IE shift from the pristine P3DDT film reached approximately +1.8 eV (from 4.4 to 6.2 eV), which is much larger than the previous result on the SSM of FC_n/PCBM (+0.35 eV above the saturated point). This could be partly explained by the fact that the density of fluoroalkyl chains on the surface is much higher in P3DDFT/P3DDT films than in FC_n/PCBM films, as described above.

To the best of our knowledge, the IE shift of +1.8 eV is the largest change induced by a molecular dipole moment even among the work function shifts observed in metal surfaces modified with highly ordered alkyl- and fluoroalkylthiol SAMs.[39−41,43−46] In a sense, the situation here is similar to that of SAMs with a mixture of alkyl and semifluoroalkyl thiols reported by Tao et al.[47] In their study, the work function of Ag was continuously shifted from 4.1 (100% alkyl thiol) to 5.8 eV (100% semifluoroakyl thiol) as the ratio of the thiols in the solution was changed. Since the dipole moments of those thiols opposed each other, the average molecular dipole moment was proportional to the thiol ratio on the surface.

Heimel et al. reported the theoretical calculations on the surface dipole effect by using poly(3-alkylthiophene)s.[26] They showed that the edge-on orientation of the polymers could induce the IE shifts of −0.4 eV for poly(3-hexylthiophene) (P3HT) and +1.8 eV for the $-CF_3$ terminated P3HT relative to the "face-on" orientation (i.e., no effect of the side chains). Although the polymer structures are different, their results suggest that the permanent dipole moments could induce the IE difference of +2.2 eV when the alkyl chains are replaced with the fluoroalkyl chains with the edge-on orientation.

Calculation of Ionization Energy Shifts. This large IE shift can be rationalized to some extent by simple electrostatic calculations of the molecules. Assuming the edge-on orientation with a perpendicular orientation of its side chains, the alkyl chains in P3DDT have a surface dipole moment pointing from the thiophene to the end of the alkyl chain. The surface segregated layer of P3DDFT would remove this dipole layer from the surface and add a new dipole moment in the opposite direction.

Dipole moment elements normal to the surface (μ) were estimated from the DFT calculations for the model compounds of P3DDT and P3DDFT, as shown in Figure 8. To simulate the symmetry breaking at the surface, the alkyl chains pointing away from the surface were removed in the models. The obtained dipole moments per unit cell were −0.84 D and +1.75 D for P3DDT and P3DDFT, respectively. The shift in the ionization energy (ΔIE) by the surface dipole layer between P3DDT and P3DDFT can be written as

$$\Delta IE = -N_{\mathrm{P3DDT}}\frac{\mu_{\mathrm{P3DDT}}}{\varepsilon_0\varepsilon_{\mathrm{r,\,P3DDT}}} - N_{\mathrm{P3DDFT}}\frac{\mu_{\mathrm{P3DDFT}}}{\varepsilon_0\varepsilon_{\mathrm{r,\,P3DDFT}}} \quad (4)$$

where ε_r represents the effective relative dielectric constant of the polymer/air interfaces, and N_{P3DDT} and N_{P3DDFT} are the surface densities of the side chains 5.50×10^{-10} mol cm^{-2} for P3DDT and 5.56×10^{-10} mol cm^{-2} for P3DDFT, respectively. However, there is an uncertainty about the relative dielectric constant (ε_r), since dipole moments exist at the surface. If the ε_r of the interfaces is assumed to be that of the corresponding side chains (ε_r, P3DDT = 2.3 from polyethylene and ε_r, P3DDFT = 2.1 from PTFE), ΔIE is +1.50 eV. If the ε_r of the interfaces is assumed to be the average of those of the side chain and air (ε_r, P3DDT = 1.65 from polyethylene/air and ε_r, P3DDFT = 1.55 from PTFE/air), ΔIE is +2.05 eV. The observed IE shift (+1.8 eV) is within this estimated range. This result supports the highly ordered orientation of semifluoroalkyl chains on the surface. To further elucidate the orientations and structures of P3DDT and P3DDFT, surface sensitive analysis such as Kelvin probe force microscopy,[48] penning ionization electron spectroscopy (PIES)[21] or near-edge X-ray absorption fine structure (NEXAFS) measurements are necessary in future studies.

CONCLUSIONS

The spontaneous formation of the surface-segregated layer of P3DDFT driven by the low surface energy of semifluoroalkyl side chains was presented. Control of the surface dipole moment induced by the layer could enable continuous control of the IE of the films depending on the concentration of P3DDFT on the surface. This layer could be regarded as a polymer semiconductor analogue to an alkylthiol SAM on metal surfaces, although its formation mechanism is completely different. The current approach has the potential to efficiently tune the energy level at the interface in various electronic devices. In fact, we recently demonstrated in a separate study that surface dipole layers can shift the relative energy level at donor/acceptor interfaces in bilayer OPVs, resulting in an increase in the open circuit voltage of such devices.[49] Thus, these polymers could be applicable to the elucidation of the fundamental relationship between the energy levels at interfaces and other various electronic processes such as the transport, generation, and recombination of charge carriers.

ASSOCIATED CONTENT

Supporting Information. XRR, AFF, and accompanying figures and tables. This material is available free of charge via the Internet at http://pubs.acs.org.

AUTHOR INFORMATION

Corresponding Authors

*E-mail: k-tajima@light.t.u-tokyo.ac.jp; hashimoto@light.t.u-tokyo.ac.jp.

Present Addresses

⊥Polymer Science and Engineering, University of Massachusetts, Amherst

Funding Sources

Funding SourcesHASHIMOTO Light Energy Conversion Project, ERATO, Japan Science and Technology Agency (JST)

ACKNOWLEDGMENT

Y.F.G. thanks the Chinese Scholarship Council for financial support. The authors thank Shoji Miyanishi for his help in the synthesis and Tomoyuki Kawai for discussion on UPS and XPS measurements.

REFERENCES

(1) Bao, Z.; Locklin, J. *Organic Field-Effect Transistors*; CRC Press: Boca Raton, FL, 2007.

(2) Salaneck, W. R.; Stafstroem, S.; Bredas, J. L. *Conjugated Polymer Surfaces and Interfaces: Electronic and Chemical Structure of Interfaces for Polymer Light Emitting Devices*; Cambridge University Press: Cambridge, U.K., 1996.

(3) Salaneck, W. R.; Seki, K.; Kahn, A.; Pireaux, J. J. *Conjugated Polymer and Molecular Interfaces: Science and Technology for Photonic and Optoelectronic Application*; Marcel Dekker: New York, 2001.

(4) Brabec, C. J.; Dyakonov, V.; Parisi, J.; Sariciftci, N. S. *Organic Photovoltaics: Concepts and Realization*; Springer: New York, 2003.

(5) Kronik, L.; Koch, N. *MRS Bull.* **2010**, *35*, 417.

(6) Shaheen, S. E.; Jabbour, G. E.; Morrell, M. M.; Kawabe, Y.; Kippelen, B.; Peyghambarian, N.; Nabor, M. F.; Schlaf, R.; Mash, E. A.; Armstrong, N. R. *J. Appl. Phys.* **1998**, *84*, 2324.

(7) Veldman, D.; Meskers, S. C. J.; Janssen, R. A. J. *Adv. Funct. Mater.* **2009**, *19*, 1939.

(8) Kobayashi, S.; Nishikawa, T.; Takenobu, T.; Mori, S.; Shimoda, T.; Mitani, T.; Shimotani, H.; Yoshimoto, N.; Ogawa, S.; Iwasa, Y. *Nat. Mater.* **2004**, *3*, 317.

(9) Pernstich, K. P.; Haas, S.; Oberhoff, D.; Goldmann, C.; Gundlach, D. J.; Batlogg, B.; Rashid, A. N.; Schitter, G. *J. Appl. Phys.* **2004**, *96*, 6431.

(10) Calhoun, M. F.; Sanchez, J.; Olaya, D.; Gershenson, M. E.; Podzorov, V. *Nat. Mater.* **2008**, *7*, 84.

(11) Martinelli, E.; Fantoni, C.; Galli, G.; Gallot, B.; Glisenti, A. *Mol. Cryst. Liq. Cryst.* **2009**, *500*, 51.

(12) Krishnan, S.; Paik, M. Y.; Ober, C. K.; Martinelli, E.; Galli, G.; Sohn, K. E.; Kramer, E. J.; Fischer, D. A. *Macromolecules* **2010**, *43*, 4733.

(13) Honda, K.; Morita, M.; Sakata, O.; Sasaki, S.; Takahara, A. *Macromolecules* **2010**, *43*, 454.

(14) Wang, Z.; Appelhans, D.; Synytska, A.; Komber, H.; Simon, F.; Grundke, K.; Voit, B. *Macromolecules* **2008**, *41*, 8557.

(15) Xue, D.; Wang, X.; Ni, H.; Zhang, W.; Xue, G. *Langmuir* **2009**, *25*, 2248.

(16) Wei, Q. S.; Tajima, K.; Tong, Y. J.; Ye, S.; Hashimoto, K. *J. Am. Chem. Soc.* **2009**, *131*, 17597.

(17) Wei, Q. S.; Nishizawa, T.; Tajima, K.; Hashimoto, K. *Adv. Mater.* **2008**, *20*, 2250.

(18) Yamakawa, S.; Tajima, K.; Hashimoto, K. *Org. Electron.* **2009**, *10*, 511.

(19) Wang, B.; Watt, S.; Hong, M.; Domercq, B.; Sun, R.; Kippelen, B.; Collard, D. M. *Macromolecules* **2008**, *41*, 5156.

(20) Li, L.; Collard, D. M. *Macromolecules* **2006**, *39*, 6092.

(21) Hao, X. T.; Hosokai, T.; Mitsuo, N.; Kera, S.; Okudaira, K. K.; Mase, K.; Ueno, N. *J. Phys. Chem. B* **2007**, *111*, 10365.

(22) Wei, Q. S.; Miyanishi, S.; Tajima, K.; Hashimoto, K. *Acs Appl. Mater. Inter.* **2009**, *1*, 2660.

(23) Wei, Q. S.; Tajima, K.; Hashimoto, K. *Acs Appl. Mater. Inter.* **2009**, *1*, 1865.

(24) Wei, Q. S.; Tajima, K.; Hashimoto, K. *Appl. Phys. Lett.* **2010**, 96.

(25) Wei, Q.; Hashimoto, K.; Tajima, K. *Acs Appl. Mater. Inter.* **2011**, *3*, 139.

(26) Heimel, G.; Salzmann, I.; Duhm, S.; Rabe, J. P.; Koch, N. *Adv. Funct. Mater.* **2009**, *19*, 3874.

(27) Cahen, D.; Kahn, A. *Adv. Mater.* **2003**, *15*, 271.

(28) Ishii, H.; Sugiyama, K.; Ito, E.; Seki, K. *Adv. Mater.* **1999**, *11*, 972.

(29) Braun, S.; Salaneck, W. R.; Fahlman, M. *Adv. Mater.* **2009**, *21*, 1450.

(30) Geng, Y. F.; Tajima, K.; Hashimoto, K. *Macromol. Rapid Commun.* **2011**, *32*, DOI: 10.1002/marc.201100275.

(31) Ton-That, C.; Shard, A. G.; Bradley, R. H. *Langmuir* **2000**, *16*, 2281.

(32) Fadley, C. S. *Prog. Sur. Sci.* **1984**, *16*, 275.

(33) Yokoyama, H.; Tanaka, K.; Takahara, A.; Kajiyama, T.; Sugiyama, K.; Hirao, A. *Macromolecules* **2004**, *37*, 939.

(34) Graupe, M.; Takenaga, M.; Koini, T.; Colorado, R.; Lee, T. R. *J. Am. Chem. Soc.* **1999**, *121*, 3222.

(35) Tsao, M. W.; Rabolt, J. F.; Schonherr, H.; Castner, D. G. *Langmuir* **2000**, *16*, 1734.

(36) Tsao, M. W.; Hoffmann, C. L.; Rabolt, J. F.; Johnson, H. E.; Castner, D. G.; Erdelen, C.; Ringsdorf, H. *Langmuir* **1997**, *13*, 4317.

(37) Heremans, P.; Janssen, D.; De Palma, R.; Verlaak, S.; Dehaen, W. *Thin Solid Films* **2006**, *515*, 1433.

(38) Sugimura, H.; Ushiyama, K.; Hozumi, A.; Takai, O. *Langmuir* **2000**, *16*, 885.

(39) Alloway, D. M.; Hofmann, M.; Smith, D. L.; Gruhn, N. E.; Graham, A. L.; Colorado, R.; Wysocki, V. H.; Lee, T. R.; Lee, P. A.; Armstrong, N. R. *J. Phys. Chem. B* **2003**, *107*, 11690.

(40) Pflaum, J.; Bracco, G.; Schreiber, F.; Colorado, R.; Shmakova, O. E.; Lee, T. R.; Scoles, G.; Kahn, A. *Surf. Sci.* **2002**, *498*, 89.

(41) Lu, J.; Delamarche, E.; Eng, L.; Bennewitz, R.; Meyer, E.; Guntherodt, H. J. *Langmuir* **1999**, *15*, 8184.

(42) de Boer, B.; Hadipour, A.; Mandoc, M. M.; van Woudenbergh, T.; Blom, P. W. M. *Adv. Mater.* **2005**, *17*, 621.

(43) Ulman, A. *Chem. Rev.* **1996**, *96*, 1533.

(44) Campbell, I. H.; Hagler, T. W.; Smith, D. L.; Ferraris, J. P. *Phys. Rev. Lett.* **1996**, *76*, 1900.

(45) Evans, S. D.; Ulman, A. *Chem. Phys. Lett.* **1990**, *170*, 462.

(46) Boudinet, D.; Benwadih, M.; Qi, Y. B.; Altazin, S.; Verilhac, J. M.; Kroger, M.; Serbutoviez, C.; Gwoziecki, R.; Coppard, R.; Le Blevennec, G.; Kahn, A.; Horowitz, G. *Org. Electron.* **2010**, *11*, 227.

(47) Wu, K. Y.; Yu, S. Y.; Tao, Y. T. *Langmuir* **2009**, *25*, 6232.

(48) Ellison, D. J.; Lee, B.; Podzorov, V.; Frisbie, C. D. *Adv. Mater.* **2011**, *23*, 502.

(49) Tada, A.; Geng, Y. F.; Wei, Q. S.; Hashimoto, K.; Tajima, K. *Nat. Mater.* **2011**, *10*, 450.